Cardiac self-gating signals for free-running imaging: more than just triggers?

Lorenzo Di Sopra[1], Jérôme Yerly[1,2], Christopher W. Roy[1], Juerg Schwitter[3], and Matthias Stuber[1,2]
[1]*Department of Diagnostic and Interventional Radiology, Lausanne University Hospital (CHUV) and University of Lausanne (UNIL), Lausanne, Switzerland,* [2]*Center for Biomedical Imaging (CIBM), Lausanne, Switzerland,* [3]*Division of Cardiology and Cardiac MR Center, Lausanne University Hospital (CHUV) and University of Lausanne (UNIL), Lausanne, Switzerland*

Synopsis

Cardiac self-gating (SG) approaches for free-running MR imaging of the heart have proven to be a robust alternative to ECG-gating. However, for both the ECG and SG signals, one feature is typically extracted (ECG: R-wave, SG: zero-crossing) and used for triggering, gating, or data binning. While this often works for constant heart rates, periods of quiescence cannot easily be predicted when heart rates change. Therefore, we have developed an algorithm that, without any prior knowledge, identifies periods of cardiac quiescence from SG signals, and demonstrated that resultant motion-suppressed image quality matches that from conventional approaches.

Introduction

Cardiac self-gating (SG) approaches for free-running MRI of the heart[1,2] have proven to be a robust and precise alternative to standard ECG gating that is based on R-wave detection.[3] However, such SG methods typically only generate temporal triggers for binning the k-space data throughout the cardiac cycle, in contrast to respiratory SG signals, whose amplitude's temporal evolution is exploited to inform binning for motion-resolved or motion-registered reconstructions.[1-5] In this study, we investigated the hypothesis that the intervals of least variability of cardiac SG signals correspond to the resting period of the cardiac cycle during diastole. To this end, free-running data sets were acquired in healthy volunteers and patients, and two methods for retrospective reconstruction of 3D static images were investigated. First, conventional mid-diastolic data subset selection and reconstruction was performed using constant window width and subject-specific time delay after the trigger point. Second, using an adaptive, non-constant window width and time delay determined by the intervals of least variability of the cardiac SG signal for each individual cardiac cycle. Timing of selected data and quality of motion-suppression in reconstructed images were then quantitatively compared for both techniques.

Methods

This IRB approved study included 9 healthy volunteers (6F, 27.4±2.4y) and 5 patients (5M, 58.2±6.1y) who provided written informed consent. All examinations were performed on a clinical 1.5T MRI scanner (MAGNETOM Aera, Siemens Healthcare, Erlangen, Germany) with a prototype bSSFP free-running (non-ECG-triggered) 3D golden-angle radial sequence with (1.15mm)^3 isotropic spatial resolution.[1,4] Both respiratory and cardiac motion signals were extracted from the imaging data with a previously reported SG technique,[1] and reconstructed as cardiac and respiratory motion-resolved 5D images using compressed sensing[3] in order to visually confirm periods of quiescent cardiac motion. 3D static images were then reconstructed with 2 different approaches, both aiming at selecting about 12% (=30%×40% along the two independent cardiac and respiratory dimensions, respectively) of all acquired readouts, corresponding to 25% of the radial Nyquist limit, similar to previous 3D radial cardiac imaging techniques.[4,6] For the first approach, a temporal window for readout selection was set with a fixed delay from the SG cardiac triggers, using the knowledge obtained from the 5D images, to reconstruct a diastolic 3D static image I_{FIXED}. For the second approach, without prior knowledge of the temporal localization of the diastolic phase within the acquired data, the defined fraction of all readouts was selected from the most quiescent portion of each cardiac cycle to reconstruct a 3D I_{ADAPT} image. To select the intervals of least variability of the cardiac SG signal c, we defined the following weighting function w_c:

$$w_c(i) = \sqrt{\left(\frac{c(i) - \bar{c}}{SD(c(i) - \bar{c})}\right)^2 + \left(\frac{c'(i)}{SD(c'(i))}\right)^2 + \left(\frac{c''(i)}{SD(c''(i))}\right)^2}$$

where i is the readout index, $\bar{c}$ is the mode of c (i.e. most frequent value of c), c' and c'' are the first and second derivatives of c, respectively, and SD is the standard deviation. The 30% of readouts with the lowest weight were then selected (Fig.1). As for respiration, for both I_{FIXED} and I_{ADAPT}, the same 40% of end-expiratory data were selected based on the respiratory SG signal amplitude as previously reported.[1-3,5] To test for consistency between the period of cardiac quiescence selected using a priori knowledge in I_{FIXED} and the automatic and adaptive selection in I_{ADAPT}, average delay and standard deviation from the corresponding cardiac SG triggers are reported. Then, image sharpness was measured for both reconstruction methods across all subjects using the slope of a sigmoid function fitted to multiple manually selected points at the left ventricular blood-myocardium interface and was statistically compared using a t-test with p<0.05 considered significant.[7]

Results

On average and across all subjects, the temporal windows with a fixed delay for I_{FIXED} reconstructions were retrospectively selected at 604±74 ms after the cardiac SG triggers, while the readouts selected for I_{ADAPT} reconstructions were found at 594±94 ms (p=0.29) (Fig.2). Conversely, the readouts selected by the fixed window showed a significantly smaller deviation from the average trigger delay than the corresponding selection from the adaptive approach (85±9 ms vs 113±14 ms, p<0.0001) (Fig.3). The left ventricular blood-myocardium interface sharpness measurements showed highly consistent results with I_{FIXED} =2.71±0.31 and I_{ADAPT} =2.71±0.34 (p=0.99) (Fig.4-5).

Discussion

The proposed data selection procedure was able to robustly identify the resting phase of the cardiac cycle from the cardiac SG signal without image-based or ECG-derived a priori knowledge. The average, dynamic trigger delay that was automatically extracted for I_{ADAPT} matched that from I_{FIXED} very closely. The only difference was found in the delay variability of selected data, which was significantly higher for I_{ADAPT} due to the automated selection procedure that dynamically adapts to the variability of individual cardiac cycle durations throughout the entire acquisition. Blood-myocardium sharpness measurements also confirmed the effectiveness of the adaptive data selection as it perfectly corroborated the values measured for the fixed-window reconstructions.

Conclusion

This study suggests that there is currently unused information in cardiac SG signals that could be exploited to maximize the quality of motion-resolution in free-running cardiac images. This may help inform an adaptive, patient-specific binning strategy throughout the cardiac cycle that aims at optimizing cardiac motion suppression for all reconstructed phases, which may be of particular benefit for clinical cohorts displaying increased heart-rate variability.

Acknowledgements

No acknowledgement found.

References

1. Di Sopra L, Piccini D, Coppo S, Stuber M, Yerly J. An automated approach to fully self-gated free-running cardiac and respiratory motion-resolved 5D whole-heart MRI. Magnetic resonance in medicine 2019;82(6):2118-2132.
2. Pang J, Sharif B, Fan Z, Bi X, Arsanjani R, Berman DS, Li D. ECG and navigator-free four-dimensional whole-heart coronary MRA for simultaneous visualization of cardiac anatomy and function. Magnetic resonance in medicine 2014;72(5):1208-1217.
3. Feng L, Axel L, Chandarana H, Block KT, Sodickson DK, Otazo R. XD-GRASP: Golden-angle radial MRI with reconstruction of extra motion-state dimensions using compressed sensing. Magnetic resonance in medicine 2016;75(2):775-788.
4. Coppo S, Piccini D, Bonanno G, Chaptinel J, Vincenti G, Feliciano H, van Heeswijk RB, Schwitter J, Stuber M. Free-running 4D whole-heart self-navigated golden angle MRI: Initial results. Magnetic resonance in medicine 2015;74(5):1306-1316.
5. Feng L, Coppo S, Piccini D, Yerly J, Lim RP, Masci PG, Stuber M, Sodickson DK, Otazo R. 5D whole-heart sparse MRI. Magnetic resonance in medicine 2017.
6. Piccini D, Littmann A, Nielles-Vallespin S, Zenge MO. Respiratory self-navigation for whole-heart bright-blood coronary MRI: methods for robust isolation and automatic segmentation of the blood pool. Magnetic resonance in medicine 2012;68(2):571-579.
7. Ahmad R, Ding Y, Simonetti OP. Edge Sharpness Assessment by Parametric Modeling: Application to Magnetic Resonance Imaging. Concepts Magn Reson Part A Bridg Educ Res 2015;44(3):138-149.

Figures

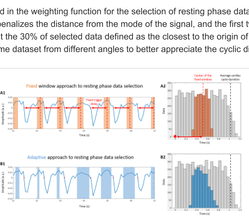

(P1) Example of the 3 dimensions considered in the weighting function for the selection of resting phase data from the cardiac SG signal (every blue dot represents a readout): the signal c itself, that penalizes the distance from the mode of the signal, and the first two derivatives, that both penalize the periods of fast cardiac motion. The green dots highlight the 30% of selected data defined as the closest to the origin of the plot (indicated by the red dot). (P2), (P3), and (P4) show the same dataset from different angles to better appreciate the cyclic distribution of weights.

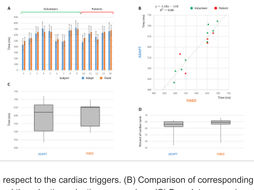

Two different strategies for data selection along the cardiac dimension. (A1) A window of fixed duration (light orange bands) is manually defined, from prior information, with a fixed delay after each cardiac trigger (red arrow and dot, respectively). (B1) The selected data (light blue bands) are automatically defined finding the intervals of least variability of the cardiac SG signal (blue), adapting to each specific cardiac cycle. Corresponding (A2) and (B2) histograms show the trigger delay of all (grey) and selected (orange/blue) readouts along the whole acquisition.

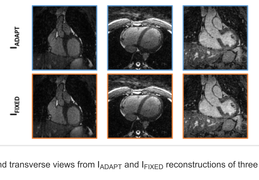

(A) Temporal delays of the selected data with respect to the cardiac triggers. (B) Comparison of corresponding average delays: the linear regression shows good agreement between the fixed window and the adaptive selection approaches. (C) Box plot summarizes the results displayed in (A), while (D) shows the corresponding results after normalization for the subject-dependent cardiac cycle mean duration. Note that only for the fixed window approach (orange) prior knowledge about the temporal position of the diastolic resting phase was used to define the selection window.

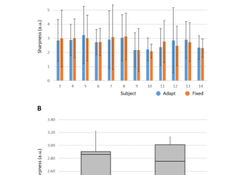

Coronal and transverse views from I_{ADAPT} and I_{FIXED} reconstructions of three datasets.

(A) Detailed overview of the measured sharpness of left ventricular blood-myocardium interface in the I_{ADAPT} and I_{FIXED} reconstructed images for 12 subjects (volunteers 1 and 2 were excluded because of image noise level), with mean and standard deviation across the selected profiles. (B) Box-plot summarizing the results of plot A with minimum and maximum values, first and third quartiles and median value.